Dissociative recombination of Ne_2^+ molecular ions

V. Ngassam* and A. E. Orel
Department of Applied Science, University of California Davis, Davis, California 95616, USA
(Received 2 December 2005; published 22 March 2006)

We present calculations of cross sections and rate coefficients for the dissociative recombination of Ne_2^+, following collisions with low-energy electrons (<1 eV). The resonance energies and autoionization widths for the doubly excited states of Ne_2 lying between the ground and first excited states of the ion are computed from electron scattering calculations using the complex Kohn variational method. The dynamics of the dissociative recombination process is investigated using multichannel quantum defect theory. The calculated absolute rate coefficient at 300 K is in good agreement with the existing measurement. The rate coefficient is found to decrease with electron temperature as $T^{-0.5}$ in the low-electron-temperature region ($T_e < 1000$ K), where the process is dominated by the lowest $^{1,3}\Sigma_g^+$ dissociative states. For the high-temperature region ($T_e > 1000$ K), where the contribution from remaining dissociative states (lowest $^{1,3}\Sigma_u^+$, $^{1,3}\Pi_g$, $^{1,3}\Pi_u$ and second resonance states of these symmetries) become more important, the rate coefficients decrease faster and eventually behave approximately as $T^{-1.5}$. We also present cross sections for competing electron-impact vibrational excitation and deexcitation of Ne_2^+ obtained from the same calculations.

DOI: 10.1103/PhysRevA.73.032720 PACS number(s): 34.80.Lx, 34.80.Ht

I. INTRODUCTION

The study of the electron–positive-ion recombination of rare-gas molecular ions,

$$e^-(\varepsilon) + R_2^+(v) \rightarrow R + R + \text{kinetic energy}, \qquad (1)$$

where R denotes a rare gas atom, was very important in the early development of the theory and mechanism of dissociative recombination and has been the subject of several experimental and theoretical investigations [1]. The interest in the dissociative recombination of rare-gas molecular ions is due to the important role they play in the ionosphere (He_2^+), gaseous lasers, plasma processing, neon lamp, and plasma displays (Ne_2^+ and Ar_2^+) and for the study of the kinematics of pulsed excimer laser sources (Ar_2^+).

A considerable amount of experimental studies for dissociative recombination of Ne_2^+ in plasma afterglow environments exist [2–6]. Most of these experiments investigated the absolute value for rate coefficients of dissociative recombination at room temperature as well as the dependence of these rates on electron and/or ion temperature. It should be noted that these experiments used two very different techniques: the stationary afterglow [2,3] where only the electrons are heated to change the temperature and the shock tube [4,6] where both the electrons and ions are heated. The shock-tube experiments lead to vibrational excitation of the ion. Therefore the cross section for dissociative recombination must be computed for different vibrational states. For the absolute value of rate coefficients at 300 K, most experiments agreed on a value between 1.7 and 2.0 $\times 10^{-7}$ cm^3 s^{-1}. However, the behavior of the rate coefficient with regard to electron temperature was found to vary from $T^{-0.5}$ to $T^{-1.5}$. These different behaviors seem to be related to the temperature of the neutral gas (from which the ion is extracted), leading to changes in the vibrational distribution of the target ion.

There exist very few theoretical studies for dissociative recombination of Ne_2^+ [7–9], giving only qualitative estimates of the cross sections and rate coefficients at room temperature as well as their variation with ion internal and electron energy. The current study has been made not only for the calculation of rate coefficients for dissociative recombination of the ($Ne_2^+ + e^-$) system, but also to understand the process of dissociative recombination for the rare-gas diatomic molecular ions. Previous calculations have described He_2^+ dissociative recombination for low [10] and high [11] electron energy, and preliminary calculations exist on the dissociative recombination of Ar_2^+ [12].

We first carried out extensive calculations of the resonance energies and autoionization widths for the doubly excited states of Ne_2 between the ground and first excited states of Ne_2^+. These are the major pathways for the dissociative recombination (DR) reaction, especially those states that cross the ion ground state near its equilibrium geometry [13]. We have also computed the Ne_2^+ ground-state potential curve as well as the low-lying Rydberg series converging to the ground state of the ion. These molecular data were then used to study the nuclear dynamics using the multichannel quantum defect theory (MQDT). Calculations were performed on an extended range of initial vibrational levels of the target ground state to allow comparison to experimental results. These have mixed vibrational ion populations which are generally assumed to follow a Boltzmann distribution law.

We also obtained cross sections for the competitive reactions of vibrational excitation and vibrational deexcitation also known as a superelastic collision (SEC):

$$e^-(\varepsilon) + R_2^+(v) \rightarrow R_2^+(v') + e^-(\varepsilon') \quad (v \neq v'), \qquad (2)$$

where R denotes a rare-gas atom.

*Electronic address: vnngassam@ucdavis.edu

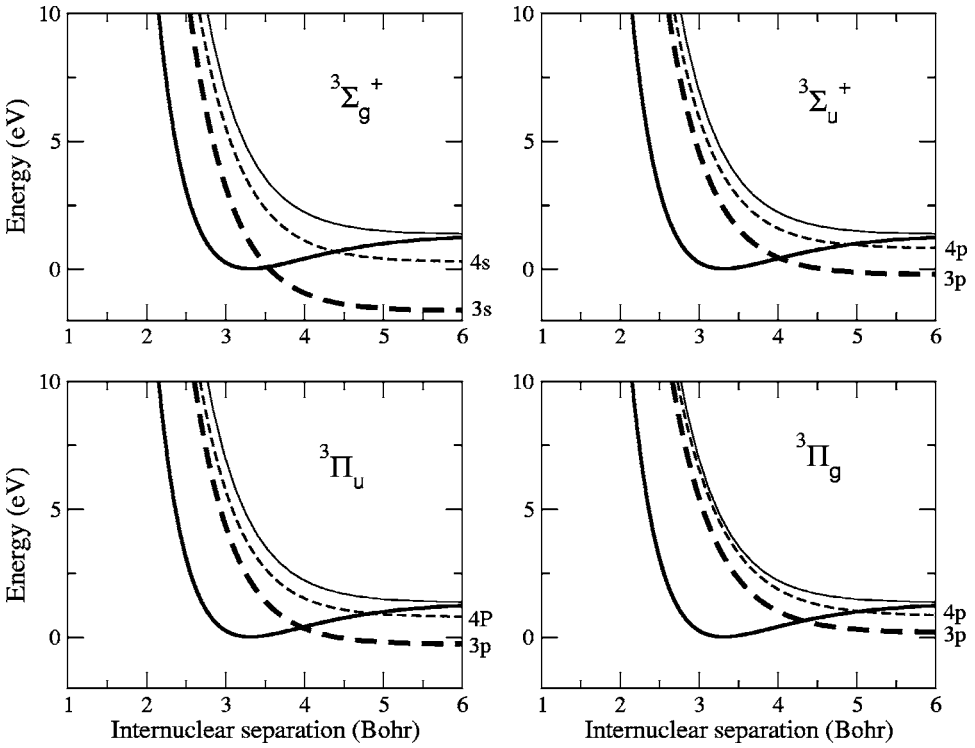

FIG. 1. Potential energy curves for the two lowest resonant $^3\Sigma_{g,u}^+$ and $^3\Pi_{g,u}$ states of Ne_2 (dashed curves) and the $^2\Sigma_u^+$ ground (bold lines) and the $^2\Sigma_g^+$ first excited (thin lines) state of Ne_2^+.

These had been shown to be dominated, as dissociative recombination, by electronic interactions which indirectly couple the vibrational states via the doubly excited states [14]

In the following sections, we will first outline the theoretical approach used in the present work; we will then present the molecular data used for the cross section calculations. Finally we will discuss the results for different initial vibrational levels of the ions and compare the behavior of the calculated rate coefficients to experimental results as well as to other theoretical predictions.

II. THEORY

A. Molecular data

Treatments of the DR process require knowledge of the potential energy curves of the ion ground state and of the doubly excited resonant states of the neutral molecule as well as the R-dependent quantum defects and electronic couplings between all the states involved. These molecular data were obtained from molecular electronic structure calculations (ground state of the ion and singly excited Rydberg states converging to the ground state of the ion) and from electron scattering calculations from the molecular ion using the complex Kohn variational method [15] to obtain resonance energies and autoionization widths of the resonant states. Additional structure calculations were necessary to continue the resonant states once they cross the ion curve.

The ground-state configuration for the neon molecular ion is

$$1\sigma_g^2 1\sigma_u^2 2\sigma_g^2 2\sigma_g^2 1\pi_u^4 1\pi_g^4 3\sigma_g^2 3\sigma_u,$$

that is, overall $^2\Sigma_u^+$ symmetry. The first-excited state $^2\Sigma_g^+$ to which the resonances converge is

$$1\sigma_g^2 1\sigma_u^2 2\sigma_g^2 2\sigma_g^2 1\pi_u^4 1\pi_g^4 3\sigma_g 3\sigma_u^2.$$

These two states go to the same asymptotic limit for large internuclear separation. To obtain the target state, we first carried out a self-consistent-field (SCF) calculation on the ion using a triple zeta plus polarization (TZP) basis set of Dunning [16]. These orbitals were then used in a multireference configuration interaction (CI) calculation, where the lowest eight orbitals were frozen and all single and double excitations from a reference space generated by a full CI for three electrons in the σ_g and σ_u occupied orbitals and the two lowest unoccupied orbitals π_{ux} and π_{uy}. This was necessary to generate a good description of the higher-lying Π states and virtual π orbitals. In order to produce a balanced treatment we used natural orbitals from averaging the density matrices for the lowest four states of the ion, $^2\Sigma_u$, $^2\Sigma_g$, and the doubly degenerate $^2\Pi_u$. Four natural orbitals $(4\sigma_g, 4\sigma_u, 2\pi_{ux}, 2\pi_{uy})$ were included as well as the occupied orbitals. The basis set was expanded to include seven additional diffuse orbitals: three s (exponents 0.1, 0.05, 0.02), three p (exponents 0.06, 0.03, 0.01), and one d (exponent 1.0). The eight lowest orbitals were frozen, and the target states were determined from a full CI in the natural orbital space (of six orbitals). The ground and first excited states of the ion are shown in Fig. 1. The equilibrium geometry and dissociation energy agree well with previous calculations [17,18].

We then carried out electron scattering calculations for low-energy electrons from the ion using the complex Kohn variational method. Since this method has been described elsewhere [15], we will only summarize it here.

In this method, the trial wave function for the $(N+1)$-electron system is expanded as

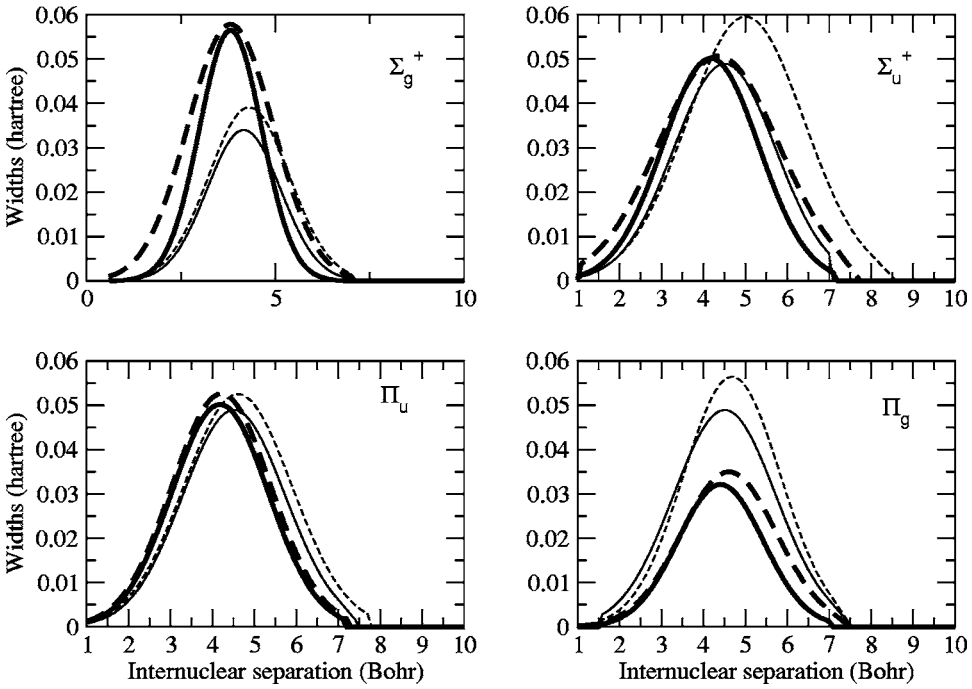

FIG. 2. Autoionization widths for the two lowest $^{1,3}\Sigma^+_{g,u}$ and $^{1,3}\Pi_{g,u}$ below the second ionization thresholds. The dashed lines represent the couplings of the triplet states; the solid lines are for the singlets. Bold lines are for the lowest resonant states while thin lines are for the second resonance states of each symmetry.

$$\Psi_{\Gamma_0} = \sum_{\Gamma} A[\Phi_{\Gamma}(\vec{r}_1, \ldots, \vec{r}_N) F_{\Gamma\Gamma_0}(\vec{r}_{N+1})] + \sum_{\mu} d_{\mu}^{\Gamma_0} \Theta_{\mu}(\vec{r}_1, \ldots, \vec{r}_{N+1}), \quad (3)$$

where the first sum (P space) usually runs over open electronic N-electron target states Γ with wave function Φ_Γ and A antisymmetrizes the coordinates of the incident electron with those of the target electrons. The second sum (Q space) contains Θ_μ which are square-integrable $(N+1)$-electron configuration-state functions (CSF's). The $(N+1)$-electron CSF's describe short-range correlation and the effects of closed channels and contain information about the resonance portion of the scattering wave function.

Two classes of terms were included in the correlation part of the wave function. The first class is the set of all $(N+1)$-electron CSF's that can be formed from the active space of target orbitals. These are generally referred to as "penetration terms" [15]. Since the scattering functions $F_{\Gamma\Gamma_0}$ are constructed from bound and continuum functions which are, by construction, orthogonal to the target orbitals, the penetration terms are needed to relax any constraints implied by this strong orthogonality. However, in addition to the penetration terms, we included a second class of "CI relaxation terms" [15]. The target ground state is built as a linear combination of a fixed number (M) of CSF's, from the active space. The target CI calculation can also produce $(M-1)$ excited states, which are presumed to be energetically closed. The CI relaxation terms are constructed as the direct product of these states and the orbitals used to describe the scattered electron. In other words, this class of CI relaxation terms is simply the complement $(1-P)$ of the P-space portion of the wave function. This complement, combined with the penetration terms, constitutes the correlation part of the trial wave function. These CI relaxation terms include the resonances which are a Rydberg series converging to the first excited state of the ion.

The addition of one electron to the $^2\Sigma^+_u$ ground state of the ion yields both singlet and triplet spin couplings and all symmetries $\Sigma_{g,u}$, $\Pi_{g,u}$, and $\Delta_{g,u}$. We performed calculations for singlet and triplet spin couplings in all symmetries at the equilibrium internuclear separation. Below the threshold for the first excited state, numerous Feshbach resonances corresponding to Rydberg series converging to the first excited state of Ne_2^+ occurred in the Σ and Π symmetries, but not in Δ. These resonances have the following configurations:

$$(1\sigma_g^2 1\sigma_u^2 2\sigma_g^2 2\sigma_g^2 1\pi_u^4 1\pi_g^4 3\sigma_g 3\sigma_u^2)^{1,3} n\lambda_{,u},$$

where λ can be σ or π.

Therefore, calculations were performed over a range of internuclear distances for only the $^{1,3}\Sigma^+_{g,u}$ and $^{1,3}\Pi_{g,u}$ symmetries. The resonance parameters (autoionization widths and resonance energies) were then extracted by fitting the eigenphase sums to a Breit-Wigner form. The two lowest resonance curves are shown in Fig. 1 for the triplet Σ and Π symmetries compared to the ion ground state. The singlet states are not represented since they were found to be similar to the triplet states. The corresponding autoionization widths for singlet and triplet states are shown in Fig. 2. For the same symmetry, the width of the triplet states is generally larger than that of the singlet, and except the Π_g symmetry, the lowest state has the most important autoionization width.

B. MQDT formalism

The two-step multichannel quantum defect theory as applied to dissociative recombination [19] and electronic autoionization [20] rests on a quasidiabatic description of molecular states [21], where two classes of electronic states,

singly excited and doubly excited, are defined. The short-range electronic interactions between states of different subspaces are then described by an electronic coupling operator **V**, which couples the ionization channels (attached to the ground-state ion core), open and closed, to dissociative ones in the case of DR or to core-excited ionization channels (or Rydberg series) in the case of electronic autoionization. From the operator **V**, a short-range reaction matrix (K matrix), a solution of a Lippmann-Schwinger integro-differential equation [22] is built:

$$\mathbf{K} = \mathbf{V} + \mathbf{V}\frac{1}{\mathbf{E} - \mathbf{H}_0}\mathbf{K}, \tag{4}$$

where $\mathbf{H}_0$ is the Hamiltonian operator excluding the electronic interaction **V**. In the case of weak coupling a perturbative solution of Eq. (4) can be obtained [19,23]. The energy dependence of the coupling can often be neglected since the electronic coupling is significant only at a short distance, where the external electron is strongly accelerated by the Coulomb attraction and thus insensitive to small differences in kinetic energy. It has been recently shown analytically that in this case, the perturbative series of Eq. (4) converges at second order [14]. To be introduce into the MQDT framework, the resulting K matrix is diagonalized:

$$\sum_j \pi K_{ij} U_{j\alpha} = -\tan\,\eta_\alpha U_{i\alpha}, \quad \alpha = 1,2,\ldots,N, \tag{5}$$

with eigenvalues $-\pi^{-1}\tan\,\eta_\alpha$ and unitary eigenvectors $U_{i\alpha}$. In the preceding equation, i and j are indexes labeling the reaction channels and N is the number of channels involved in the calculation. The eigenvalues $-\pi^{-1}\tan\,\eta_\alpha$ and the eigenvector elements $U_{j\alpha}$ are used in a frame transformation to build the channel-coupling coefficients for the MQDT treatment of DR and electron-impact vibrational transitions, i.e.,

$$\mathcal{C}_{v\alpha} = \sum_{v'} U_{v'\alpha}\langle v|\cos[\pi\mu(R) + \eta_\alpha]|v'\rangle_R, \tag{6}$$

$$\mathcal{C}_{d\alpha} = U_{d\alpha}\cos\,\eta_\alpha, \tag{7}$$

$$\mathcal{S}_{v\alpha} = \sum_{v'} U_{v'\alpha}\langle v|\sin[\pi\mu(R) + \eta_\alpha]|v'\rangle_R, \tag{8}$$

$$\mathcal{S}_{d\alpha} = U_{d\alpha}\sin\,\eta_\alpha, \tag{9}$$

where v and v' designate the vibrational states of the molecular ion, d is the dissociative channel, and the integration $\langle\cdots\rangle_R$ is over the internuclear distance. Note that the nonadiabatic radial coupling between two ionization channels v and v' is introduced here through the R dependence of the quantum defect μ. Indeed, a constant quantum defect results in all nondiagonal $v \neq v'$ terms from Eqs. (6) and (8) vanishing and thus decouples the ionization channels.

The last step of the MQDT treatment is the construction of the asymptotic scattering matrix and the calculation of the cross sections. We follow the method of Seaton [24] as first applied by Nakashima *et al.* [25] to the treatment of DR and related processes. The matrices $\mathcal{C}$ and $\mathcal{S}$ are used to build the "generalized" scattering matrix **X** which involves the whole set of channels, open or closed, for ionization or dissociation:

$$\mathbf{X} = \frac{\mathcal{C} + i\mathcal{S}}{\mathcal{C} - i\mathcal{S}}. \tag{10}$$

Then, the physical scattering matrix **S** is calculated by elimination of the closed channels:

$$\mathbf{S} = \mathbf{X}_{oo} - \mathbf{X}_{oc}\frac{1}{\mathbf{X}_{cc} - e^{-2i\pi\nu_v}}\mathbf{X}_{co}. \tag{11}$$

The index o (c) means open (closed) channel blocks. The parameters $\nu_v = 1/\sqrt{2(E_v - E)}$, analogous to the effective quantum number of a Rydberg level, are defined for each closed channel with threshold energy E_v higher than the total energy E.

Finally, for the initial ion level v and for a multiplicity ratio g between the ion and dissociative states, the cross sections are given by

$$\sigma_{dv} = \frac{\pi}{2\varepsilon}\frac{g}{2}|S_{dv}|^2 \tag{12}$$

for dissociative recombination and by

$$\sigma_{v'v} = \frac{\pi}{2\varepsilon}\frac{g}{2}|S_{v'v}|^2 \tag{13}$$

for superelastic collisions ($v' < v$) or vibrational excitation ($v' > v$).

C. Calculation of rate coefficients

To obtain the rate coefficients, the theoretical cross sections are convoluted with an instrumental function to simulate the experimental conditions. In the case of afterglow experiments, the convoluted rate coefficient $\alpha_v(T_e)$ for each initial vibrational level of the target ion can be obtained by averaging over an isotropic Maxwell-Boltzmann distribution of electron energies:

$$\alpha_v(T_e) = \int \sigma_v(\epsilon)\epsilon f(\epsilon)d\epsilon, \tag{14}$$

where $\sigma_v(\epsilon)$ is the calculated cross section as a function of the collision energy for the initial vibrational level v of the ion. The function $f(\epsilon)$ is the Maxwell-Boltzmann function given by

$$f(\epsilon) = \frac{8\pi m_e}{(2\pi m_e kT_e)^{3/2}}\exp\left(-\frac{\epsilon}{kT_e}\right), \tag{15}$$

where m_e is the electron mass, k is the Boltzmann constant, and ϵ is the electron energy.

The final rate coefficient as a function of electron temperature is then obtained by averaging the above-mentioned rates over the various initial vibrational levels according to their population at a given gas temperature,

$$\alpha(T_e) = \sum_v \alpha_v(T_e)\frac{n_v}{N}, \tag{16}$$

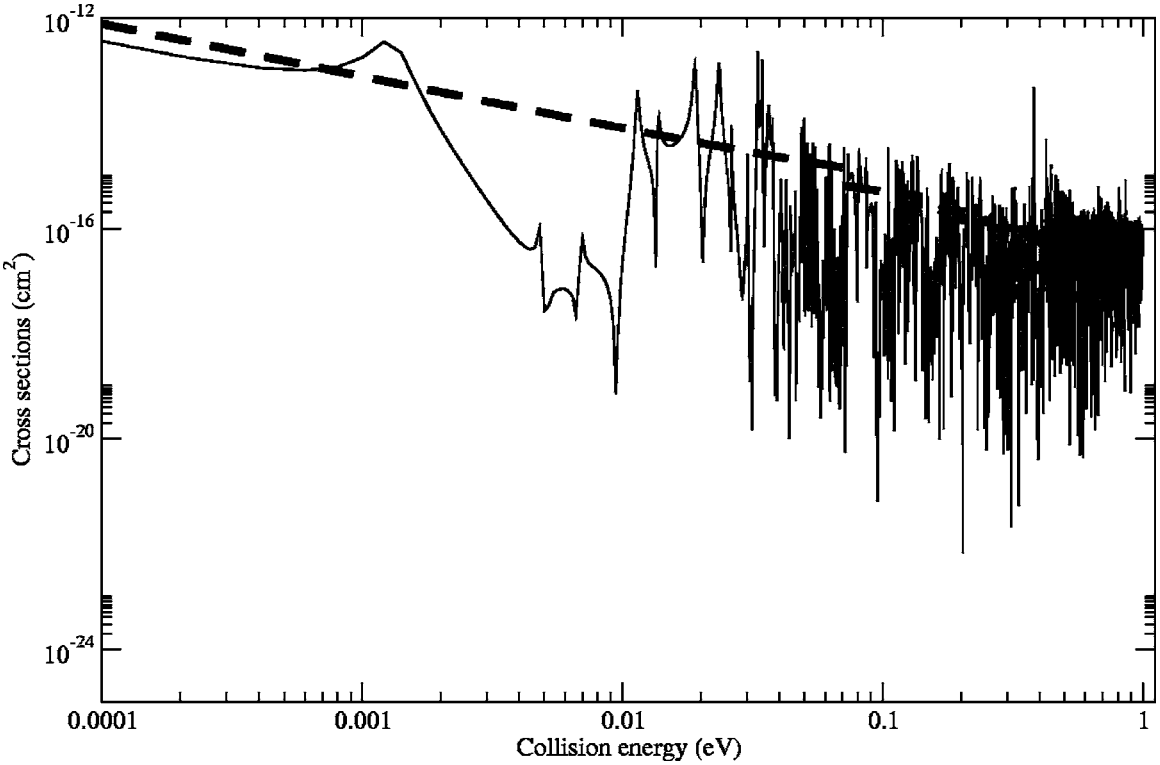

FIG. 3. Cross section for dissociative recombination of Ne_2^+ via the $^3\Sigma_{g,u}^+$. The dashed line represent the direct process. The solid line is the total process (direct+indirect).

where n_v is the population of the vibrational level v_i at a given gas temperature assuming a Boltzmann distribution of vibrational populations and N is the total ion population.

III. RESULTS AND DISCUSSION

The dissociation dynamics was studied using the multichannel quantum defect theory [19] with a second-order K matrix [26]. In the present case, where there is one or more repulsive resonant states which cross the ion ground state near the equilibrium geometry, the dissociative recombination has been shown to be dominated by the direct process where the electron is capture in one of these resonant states. As an example, we compare the direct and the total (direct +indirect) cross sections for dissociative recombination of the ground vibrational state ($v=0$) via the lowest $^1\Sigma_g^+$ resonant state in Fig. 3. This state will be shown later to be the most important route for low-energy dissociative recombination of Ne_2^+. Note that the quantum defects used for the combined calculation are approximate and the results are just illustrative. As can be seen in this figure, introducing the indirect process leads to cross sections with complicated resonance structure at low energies, due to interfering series of resonances, but will not have noticeable effects on the averaged magnitude and behavior of the cross section. For the case of the lowest $^1\Sigma_g^+$ shown in Fig. 3 we have compared the thermal rate coefficients obtained from the two calculations. The inclusion of the indirect process does slightly lower the magnitude of the rate coefficients but it does not modify the temperature dependence for the rate coefficients. In this case the resonant states cross the ion near its equilibrium geometry and the direct mechanism is very strong. Therefore, the effects of indirect meachanism are much smaller than the direct. This difference in magnitude between the two calculations decreases for higher vibrational states. Therefore, we did not included the Rydberg bound states responsible for the "indirect" DR process in the calculations. Rotational effects were not included as well since they are not taken into account in the existing experiments. Also, these effects were shown to be negligible when the direct process based on a strong electronic interaction is fast and dominant, especially for heavier ions like Ne_2^+ [27].

A. Partial cross sections

Ne_2^+ has 32 bound vibrational levels. It was necessary to calculate the absolute cross sections up to the 21st vibrational level in order to study a range of electron and gas energies varying up to 1 eV. All the symmetries in which resonant states were found ($^{1,3}\Sigma_{g,u}^+$ and $^{1,3}\Pi_{g,u}$) were included in the calculations as they became open in energy. As can be seen in Fig. 1 scattering in $^{1,3}\Sigma_g^+$ yields resonances that lie only about 1 eV above the ground state of the ion and which cross the ion potential energy curve just above the $v=0$ vibrational level. The interactions of the lowest states of this symmetry with the ionization continuum, represented in Fig. 2 by the autoionization widths, are comparable to those of the other symmetries. The lowest $^{1,3}\Sigma_g^+$ resonant states were thus anticipated to be the major pathways for dissociative recombination of Ne_2^+ following impact with low-energy

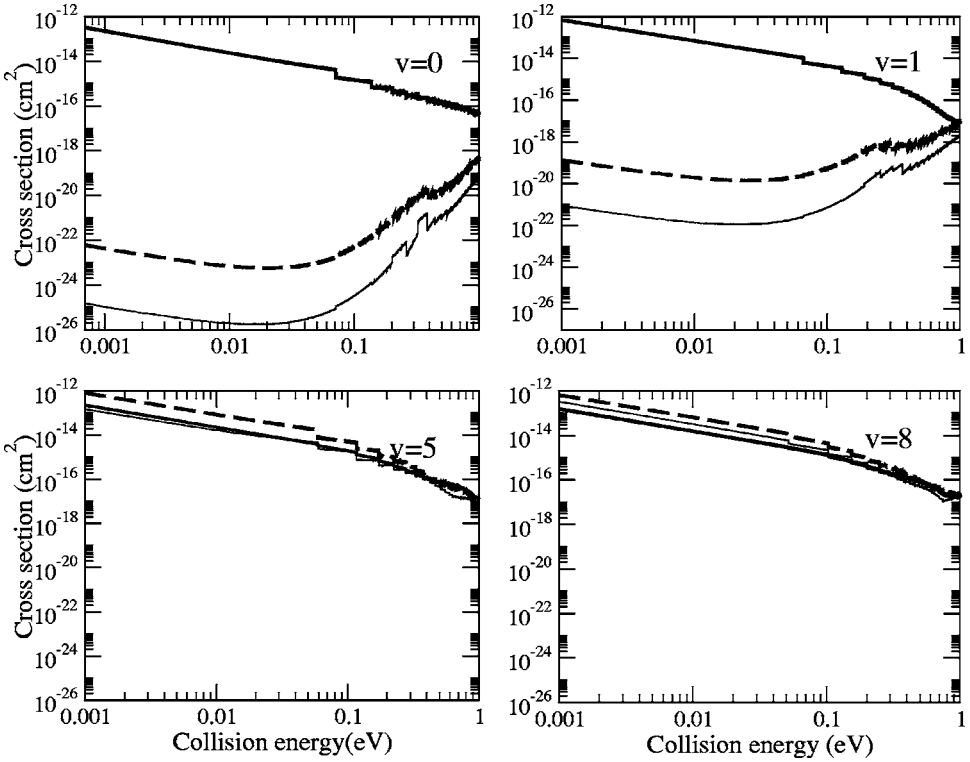

FIG. 4. Partial cross section for dissociative recombination of Ne_2^+ initially in $v=0$, 1, 5, and 8. The bold lines represent the $^3\Sigma_g^+$ partial cross sections, while the thin and dashed lines are, respectively, the $^3\Sigma_u^+$ and $^3\Pi_u$ contributions to the cross section.

electrons, with the contribution of the other symmetries ($^{1,3}\Pi_u$, $^{1,3}\Sigma_u^+$, $^{1,3}\Pi_g$) becoming more important and eventually dominating as the vibrational energy of the target state and/or the electron energy is increased. The lowest singlet and triplet Π_g states were not energetically open at low energy for the lower vibrational levels ($v<10$).

We compare the cross sections for dissociative recombination via the lowest resonant states of the various symmetries, in Fig. 4 for the low vibrational states ($v<10$) and in Fig. 5 for the high vibrational states of the ion. With few exceptions generally due to very small Franck-Condon overlaps, the cross sections calculated fall off as the inverse of the collision energy. The steps seen in the cross sections correspond to the opening of new vibrational channels, allowing new routes for autoionization which competes with dissociative recombination.

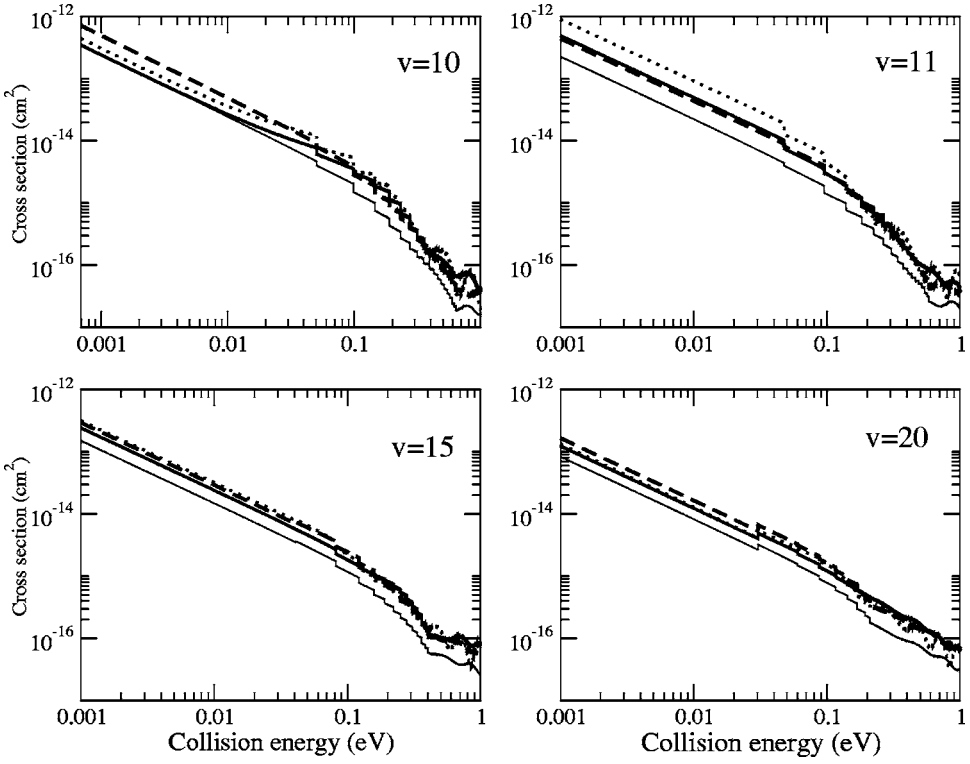

FIG. 5. Same as Fig. 4 for $v=10$, 11, 15, and 20. The contribution of the Π_g states which is now opened for dissociation at "zero" energy is represented by the dotted lines.

As discussed above and as can be seen in Fig. 4 ($v=0$ and $v=1$), the low-energy recombination cross section is dominated by the lowest $^{1,3}\Sigma_g^+$ resonances, which both have a better overlap of the wave function with that of the electronic continuum. In the same figure, the $^{1,3}\Pi_u$ and $^{1,3}\Sigma_u^+$ contributions to the cross sections are both negligible at very low energy. These contributions increase with electron energy and become comparable with the $^{1,3}\Sigma_g^+$ partial cross section around 1 eV. For $v=5$ and greater (Fig. 4, $v=5$ and $v=8$), all symmetries contribute almost equally to the cross section for the whole range of electron energies calculated, the Π_u symmetry being the most important. At $v=10$ the first dissociative state of the $^{1,3}\Pi_g$ symmetry as well as the second resonance states for the other symmetries open for dissociation at "zero" energy and are included in the calculation. The partial cross sections fluctuate depending on the importance of the Franck-Condon factor between the resonant-state wave function and the wave function of the initial vibrational state, but remain at the same order of magnitude with the increasing internal energy of the ion (see Fig. 5). Note that since the resonance energies for the singlet and triplet states of the same symmetry are similar and the autoionization widths are not dramatically different, the cross sections for the triplet states are roughly 3 times those for the singlet states of the same symmetry; i.e., the difference is only due to the multiplicity of the states. Also, the contributions of the Π states are generally higher than those of the Σ states.

The total cross section for each vibrational level is obtained by summing the contribution of all the dissociative states involved at each energy. From the total cross section, the rate coefficients will be obtained and analyzed, and compared to available experimental data.

B. Rate coefficients for DR

All the experimental studies of Ne_2^+ dissociative recombination have been performed using afterglow techniques [28]. In these types of experiments, the recombination rate coefficients are generally determined from the decay of the electron density with time following the removal of the external ionizing source. Most experiments [2,3] were performed over a restricted range of gas (ion) temperatures ($T_g < 500$ K). These experiments found the rate coefficients for dissociative recombination of Ne_2^+ with a temperature dependence close to $T^{-0.5}$ over a range of electron temperature between 300 K and 10^4 K in accordance with the Wigner threshold law [29]. More recently, Chang *et al.* [6] measured the rate coefficients for dissociative recombination of Ne_2^+ at elevated gas and electron temperatures using a shock-heated pulsed-flow rf-discharge pulsed afterglow. The variation of the rate coefficients was shown to be between $T^{-0.6}$ and $T^{-1.0}$ for elevated gas temperatures of, respectively, 2200 K and 2700 K. This changes to approximately $T^{-1.5}$ when the electron and gas temperatures were kept equal but above 1500 K, in qualitative agreement with the results of Cunningham and Hobson [4]. This rather unusual temperature dependence was supported by the earlier works of Cunningham and co-workers [4,9], which predict a breakdown in the slope of the rate coefficient for dissociative recombination of rare-gas diatomic ions (around 900 K for Ne_2^+) as a function of electron energy, leading to $T^{-1.5}$ in the high-temperature region. The first attempt to explain this fast decrease of rate coefficients with increasing temperature based on the importance of the indirect mechanism was suggested by Chen and Mittleman [30] and Bardsley [31]. A year later, Bardsley [32] showed that the indirect process gives rate coefficients that decrease as $T^{-1.5}$ and that the actual temperature dependence of the rate coefficients of dissociative recombination should depend on the relative strength of the two mechanisms. However, he treated the two processes independently, thus neglecting the interferences between them since there occur together. Another attempt to explain the $T^{-1.5}$ behavior of the rate coefficients was made by O'Malley and co-workers [33] with a "low-vibrational-state" (LVS) model. However, this model is based on a single resonant state description of dissociative recombination, with the resonant state crossing the ion so that the cross section is maximum for a low vibrational state $v=0-2$.

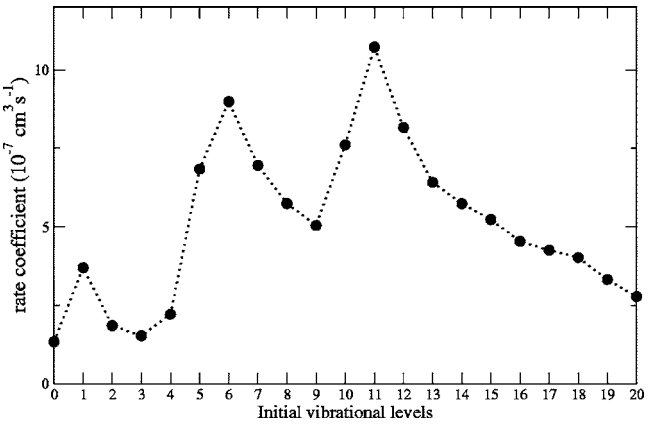

FIG. 6. Rate coefficients for dissociative recombination of Ne_2^+ at fixed electron temperature of 300 K (corresponding to a collision energy of 0.026 eV) as a function of the initial vibrational states of the ion.

In order to compare our results with existing measurements, the theoretical cross sections were converted into rate coefficients after a convolution with an isotropic Maxwell-Boltzmann distribution of electron energies and averaged over the initial vibrational states populated at a given gas and ion temperature as in Eqs. (14) and (16). Figure 6 displays the rate coefficients at fixed electron temperature of 300 K corresponding to a collision energy of 0.026 eV for various initial vibrational levels of the ion. The rate coefficients fluctuate with the initial vibrational energy level. This behavior can be explained by the relative contribution from various resonant states for different initial vibrational levels. The peak at $v=1$ is due to a good overlap of the wave function of the first vibrational excited state ($v=1$) of the ion with the lowest $^{1,3}\Sigma_g^+$ resonant state. Then, this lowest $^{1,3}\Sigma_g^+$ dominant contribution drops dramatically, and around $v=6$, the contributions of the lowest $^{1,3}\Pi_u$ and $^{1,3}\Sigma_u^+$ contribution to the process become more important, once more due to a good overlap of the wave functions. The last peak is due to the opening of new routes for dissociative recombination (lowest $^{1,3}\Pi_g$ and second resonant states of the other symmetries).

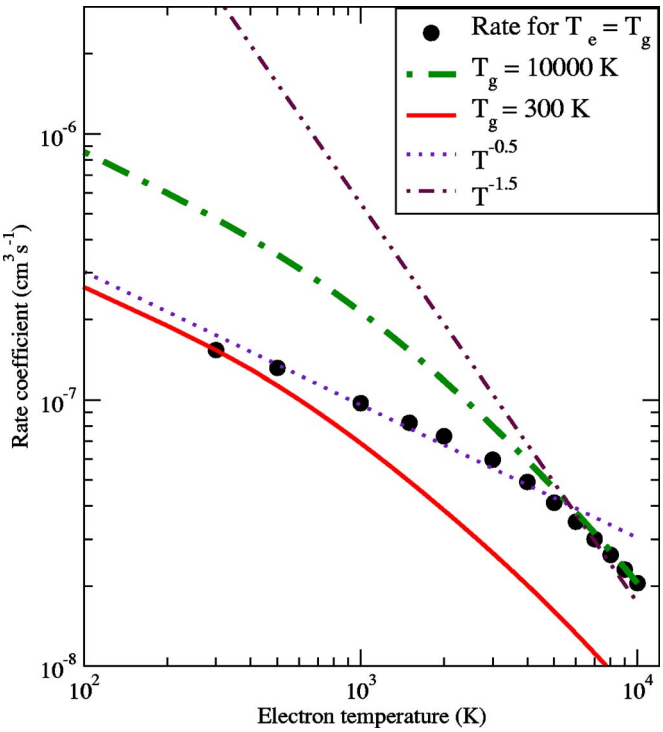

FIG. 7. (Color online) Calculated rate coefficients for dissociative recombination of Ne_2^+ as a function of the electron temperature for various gas temperatures. The dotted and dash–double-dotted lines shown represent, respectively, the slope of the $T^{-0.5}$ and $T^{-1.5}$ temperature dependences.

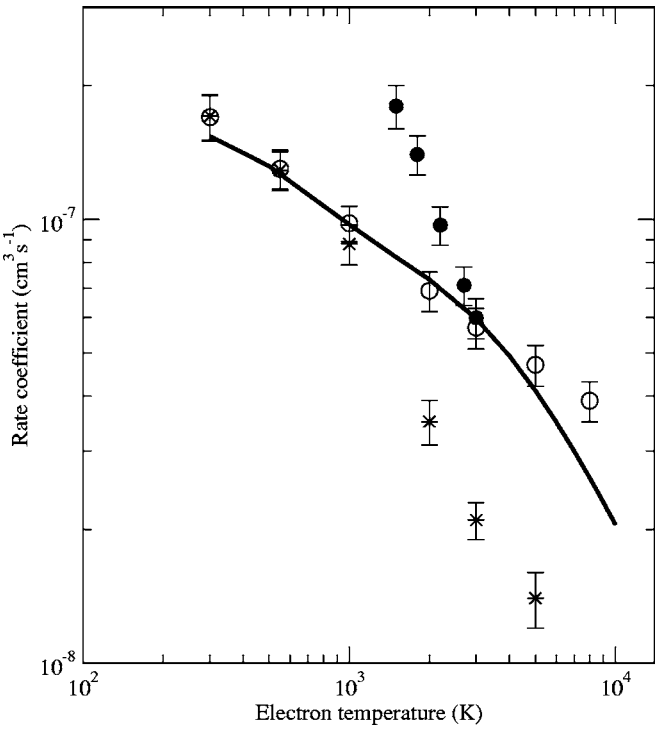

FIG. 8. Comparison of the calculated rate coefficients for dissociative recombination of Ne_2^+ with various experiments. The solid line represents the theoretical rate coefficients for $T_g = T_e$. The open circles are measurements of Frommhold *et al.* [2] at 300 K. The stars represent the results of Cunningham and Hobson [4], while the solid circles are measurements of Chang *et al.* [6], both performed with $T_g = T_e$.

The rate coefficient for dissociative recombination at 300 K arises primarily from a contribution of the two lowest vibrational states ($v=0$ and $v=1$). The theoretical value is 1.503×10^{-7} cm^3 s^{-1}, in good agreement with most experiments which report a rate coefficient of $(1.7 \pm 0.2) \times 10^{-7}$ cm^3 s^{-1} [6].

The absolute rate coefficients for dissociative recombination, at a fixed gas temperature (300 K, 10 000 K) and for a gas temperature always equal to the electron temperature, as a function of electron temperature are displayed in Fig. 7. Also shown are the lines representing slopes of $T^{-0.5}$ and $T^{-1.5}$. At 300 K, the rate coefficients decrease as $T^{-0.5}$ for low electron temperature. This behavior of the rate coefficients at low energy can be explained by the fact that at these energies the process is always dominated by a single resonance and the cross sections then follow the Wigner threshold law [29]. As the electron temperature increases, new routes for dissociative recombination open causing a deviation from the $T^{-0.5}$ behavior around 700 K. At elevated gas temperature (10 000 K), the rate coefficients are higher at low electron energy since many resonant states contribute to the process even at low electron temperature and the high vibrational states dissociate faster. At these temperatures, the rate also decreases faster than $T^{-0.5}$ even at low energy. When the electron temperature is kept equal to the gas temperature, the rate decreases as $T^{-0.5}$ at low energy with a break in the slope after 2000 K. Then the rate coefficient decreases faster and eventually as approximately $T^{-1.5}$. The break observed in the rate coefficients as a function of electron and gas temperatures is clearly displayed in the experimental data of Cunningham and Hobson [4] shown in Fig. 8 (star). Here, we also plot theoretical rate coefficients with the gas temperature always equal to the electron temperature as in the experiment. At low energies, there is a very good agreement between theory and the Cunningham-Hobson experiment as well as with the experiment performed at a fixed gas temperature (300 K) [2] and represented by the open circles. For higher energies, unlike experimental results, theoretical rate coefficients go from the $T^{-0.5}$ behavior to approximately the $T^{-1.5}$ smoothly. In absolute values, the theoretical rate coefficients are closer to the most recent experiment done at elevated electron and gas temperatures [6]. Using the model of O'Malley *et al.*, the smooth change in the behavior of the present theoretical rate coefficients compared to experiment might be explained by the fact that our cross section for dissociative recombination is most important around $v=10$ rather than $v=1$ as assumed by O'Malley *et al.*

C. Rate coefficients for electron-impact vibrational excitation and deexcitation

Cross sections for electron-impact vibrational excitation and deexcitation (SEC) can be obtained from the same scattering matrix used to calculate the DR cross section, but corresponding to different matrix elements. In the case of a single resonant doubly excited state, for example, and using

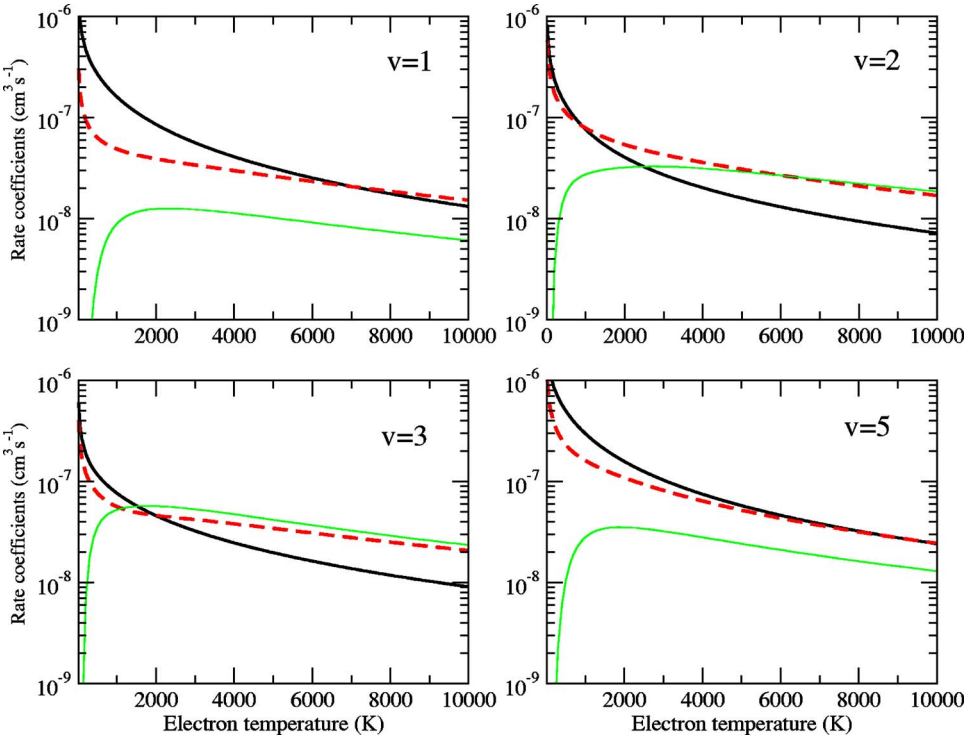

FIG. 9. (Color online) Rate coefficients for vibrational excitation (solid grey line) and deexcitation (dashed line) of Ne_2^+ for $\Delta v=1$ compared to the rate coefficients for dissociative recombination (solid dark line) initially in $v=1$, 2, 3, 5 vibrational states.

the first-order perturbation for the K matrix, the matrix elements S_{dv} and $S_{v'v}$ of Eqs. (12) and (13) are given, respectively, by

$$S_{dv} = -2i\frac{\xi_v}{1+\xi^2} \tag{17}$$

and

$$S_{v'v} = -2\frac{\xi_v \xi_{v'}}{1+\xi^2}, \tag{18}$$

where $\xi_v = \pi \int \chi_v(R) V_{el}(R) F_d(R) dR$ and $\xi^2 = \Sigma_v \xi_v^2$.

There have been no experimental determination of cross sections or rate coefficients for vibrational excitation and deexcitation of Ne_2^+. Therefore, the data obtained in the current study will be useful for the modeling of plasmas where Ne_2^+ is abundant. We have computed cross sections for vibrational excitation and deexcitation of Ne_2^+ up to $v=20$ initial vibrational levels. Here, we will only discuss the results for the six lowest initial vibrational levels of the ion. The rate coefficients for vibrational excitation and SEC of Ne_2^+ initially in $v=1$, 2, 3, and 5 vibrational states are shown in Fig. 9 for the transitions with $\Delta v=1$. These results display two interesting features. First the rate coefficients for vibrational transitions have the same pattern as those of dissociative recombination at very low electron temperatures. As the electron temperature increases, the rate coefficients for dissociative recombination decrease faster than those of vibrational excitation and deexcitation; this is due to the fact that one of the vibrational states involved in the vibrational transitions has a better overlap with the resonant state involved for these high energies. Note that that the transitions involving the $v=1$ and $v=5$ vibrational states are faster than the others. As shown in Fig. 6 for low vibrational levels ($v<10$), the $v=1$ and $v=5$ have the highest dissociative recombination rate coefficients, suggesting that as in H_2^+ the processes are driven by the same mechanism through the dissociative resonant state. Second, except for the rapid rise from the threshold, the rate coefficients for vibrational excitation and SEC have the same order of magnitude for the same initial vibrational state but are always smaller than those of dissociative recombination at low electron temperature. These results are contrary to the case of H_2^+ where the superelastic collision was shown to be faster than dissociative recombination [14,34]. The case of $v=1$ and $v=5$, where the rate coefficients for vibrational excitation are much smaller than those of DR and SEC, can be explained by the weak overlap of the wave functions of $v=2$ and $v=6$, which are involved in these excitations, with the wave function of the dissociative resonant state. Figure 10 shows the rate coefficients of vibrational transitions for $v=4$ initial vibrational states of the ion and different transitions Δv in comparison with rate coefficients of dissociative recombination. With the exception of the transitions involving the $v=1$ vibrational state, at low energy, the rate coefficient decreases as Δv increases, but the transitions with $\Delta v \neq 1$ are not negligible compared to those with $\Delta v=1$. This behavior is quite similar for the other vibrational states. One of the most important points here, as in DR, is how efficient the transition between the vibrational states involved and the resonant states which govern the processes becomes. The transitions with $\Delta v \neq 1$ must be taken into account to accurately model plasmas where Ne_2^+ is abundant.

D. Final atomic states

All the resonant states included in the present calculation correlate with one neon atom in the ground state and the other in a metastable state $(nl)^{1,3}$ with $n=3$ or 4 and $l=s$, p,

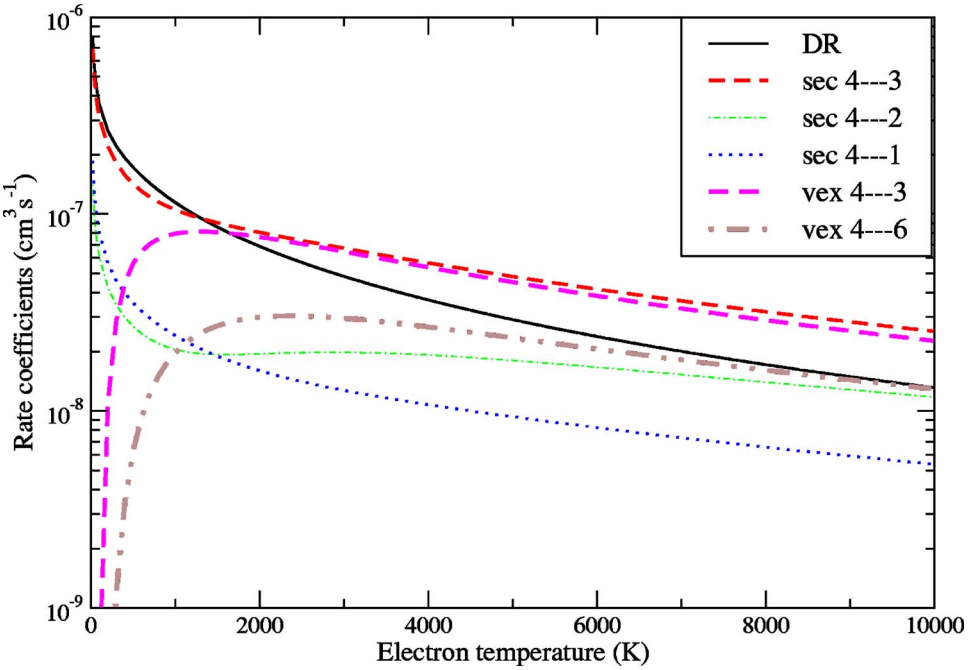

FIG. 10. (Color online) Rate coefficients for vibrational excitation and deexcitation of Ne_2^+ initially in the $v=4$ vibrational level. All transitions $|\Delta v|$ are shown. DR rate coefficients are also shown.

or *d*. There exists an infinite series of singly excited Rydberg states of Ne_2 converging to the $^2\Sigma_u^+$ ground state of Ne_2^+. These states couple to the resonant states of the same symmetry, which can lead to a redistribution of the flux between different final atomic states. This flux redistribution depends on the strength of the electronic couplings between the resonant states and the singly excited Rydberg states. In the calculations on He_2^+ [11], these crossings were not found to significantly affect the branching ratios; therefore, such states are not included in the present calculation. The final-state distribution also depends on the initial vibrational state of the molecular ion since this, with the electron energy, will determine which resonant states are populated after the electron is captured and thus which final atomic states are formed.

For the low vibrational states at very low electron energy dissociative recombination proceeds through the lowest resonant states which correlate to $n=3$. As the electron energy increases to approximately 1 eV, some states that dissociate into $n=4$ contribute, but the percentage of $n=4$ atoms remain negligible compared to the $n=3$ states. As the vibrational energy of the ion increases, the second resonant states of various symmetries correlated to the $n=4$ atomic states become more important but never dominate.

IV. CONCLUSION

We have computed rate coefficients for dissociative recombination for the Ne_2^+ molecular ion with low-energy electrons as a function of electron and gas temperatures. The dissociative recombination rate coefficients obtained at room temperature (300 K) are in good agreement with the various measurements in afterglow devices. The rate coefficients decrease as $T^{-0.5}$ at low temperature and approximately as $T^{-1.5}$ at high temperature, in good agreement with very recent measurements. However, the break in the slope of theoretical rate coefficients occurs at higher energy compared to experiments.

The rate coefficients for vibrational excitation and deexcitation were also presented. These processes are driven by the same mechanism as DR. The rate coefficients for vibrational excitation and deexcitation are lower than those of dissociative recombination with the same initial vibrational levels and decrease when Δv increases. Since no experimental rate coefficients for vibrational excitation and deexcitation exist, these can be very useful in modeling of Ne_2^+ plasma.

ACKNOWLEDGMENTS

We thank R. Johnsen, O. Motapon, I. F. Schneider, and A. Suzor-Weiner for useful discussions. We acknowledge support from the National Science Foundation under Grant No. PHY-02-44911. Part of this work was performed under the auspice of the NATO Science programme through Collaborative linkage Grant No. PST.GLG.9794033.

[1] M. A. Biondi, in *Dissociative Recombination of Molecular Ions with Electrons*, edited by S. L. Guberman (Kluwer Academic/Plenum, New York, 2003), p. 13.
[2] L. Frommhold, M. Biondi, and F. J. Mehr, Phys. Rev. **165**, 44 (1968).
[3] W. H. Kasner, Phys. Rev. **167**, 148 (1968).
[4] A. J. Cunningham and R. M. Hobson, Phys. Rev. **185**, 98 (1969).

[5] J. Philbrick, F. J. Mehr, and M. Biondi, Phys. Rev. **181**, 271 (1969).
[6] J. S. Chang, R. M. Hobson, Y. Ichikawa, T. Kaneda, N. Maruyama, and S. Teii, J. Phys. B **22**, L665 (1989).
[7] C. S. Warke, Phys. Rev. **144**, 120 (1966).
[8] R. L. Wilkins, J. Chem. Phys. **44**, 1884 (1966).
[9] A. J. Cunningham, T. F. O'Malley, and R. M. Hobson, J. Phys. B **14**, 773 (1981).
[10] L. Carata, A. E. Orel, and A. Suzor-Weiner, Phys. Rev. A **59**, 2804 (1999).
[11] J. Royal and A. E. Orel, Phys. Rev. A **72**, 022719 (2005).
[12] J. Royal and A. E. Orel, Phys. Rev. A (unpublished).
[13] D. R. Bates and H. S. W. Massey, Proc. R. Soc. London, Ser. A **170**, 261 (1947).
[14] V. N. Ngassam, O. Motapon, A. Florescu, L. Pichl, I. F. Schneider, and A. Suzor-Weiner, Phys. Rev. A **68**, 032704 (2003).
[15] T. N. Rescigno, B. H. Lengsfield, and C. W. McCurdy, in *Modern Electronic Structure Theory*, edited by D. R. Yarkony (World Scientific, Singapore, 1995), Vol. 1, p. 501.
[16] T. H. Dunning, Jr., J. Chem. Phys. **55**, 716 (1971).
[17] F. Y. Naumkin and D. J. Wales, Med. Prog. Technol. **93**, 633 (1998).
[18] E. C. M. Chen and E. S. Chen, Chem. Phys. Lett. **293**, 491 (1998).
[19] A. Giusti-Suzor, J. Phys. B **13**, 3867 (1980).
[20] A. Giusti-Suzor and H. Lefebvre-Brion, Chem. Phys. Lett. **76**, 132 (1980).
[21] V. Sidis and H. Lefebvre-Brion, J. Phys. B **4**, 1040 (1971).
[22] R. D. Levine, *Quantum Mechanics of Molecular Rate Processes* (Clarendon, Oxford, 1969).
[23] S. L. Guberman and A. Giusti-Suzor, J. Chem. Phys. **95**, 2602 (1991).
[24] M. J. Seaton, Rep. Prog. Phys. **46**, 167 (1983).
[25] K. Nakashima, H. Takagi, and H. Nakamura, J. Chem. Phys. **86**, 726 (1986).
[26] V. Ngassam, A. Florescu, L. Pichl, I. F. Schneider, O. Motapon, and A. Suzor-Weiner, Eur. Phys. J. D **26**, 165 (2003).
[27] B. Vâlcu, I. F. Schneider, M. Raoult, C. Strömholm, M. Larsson, and A. Suzor-Weiner, Eur. Phys. J. D **1**, 71 (1998).
[28] J. B. A. Mitchell, Phys. Rep. **186**, 215 (1990).
[29] E. P. Wigner, Phys. Rev. **73**, 1002 (1948).
[30] J. C. Y. Chen and M. H. Mittleman (unpublished).
[31] J. N. Bardsley (unpublished).
[32] J. N. Bardsley, J. Phys. B **1**, 365 (1968).
[33] T. F. O'Malley, A. J. Cunnigham, and R. M. Hobson, J. Phys. B **5**, 2126 (1972).
[34] S. Krohn, Z. Amitay, A. Baer, D. Zajfman, M. Lange, L. Knoll, J. Levin, D. Schwalm, R. Wester, and A. Wolf, Phys. Rev. A **62**, 032713 (2000).